Journal of Robotics and Control (JRC)
Volume 6, Issue 1, 2025
ISSN: 2715-5072, DOI: 10.18196/jrc.v6i1.23953

Design and Simulation of a 2-Degree of Freedom Energy Harvester from Blood Flow for Powering the Pacemaker

Manar Abdelmawgoud [1*], Victor Parque [2], Ayman Nada [3], Ahmed M. R. Fath El-Bab [4]
[1,3,4] Department of Mechatronics and Robotics Engineering, Egypt-Japan University of Science and Technology (E-JUST), Alexandria 21934, Egypt
[2] Graduate School of Advanced Science and Engineering, Hiroshima University, Japan
Email: [1] mannar.abdelmawgoud@ejust.edu.eg, [2] parque@hiroshima-u.ac.jp, [3] ayman.nada@ejust.edu.eg, [4] ahmed.rashad@ejust.edu.eg
*Corresponding Author

***Abstract*—The pacemaker is a device that is used to treat different abnormal heart rhythms. It is usually powered using traditional batteries. These batteries run out of power after about 7 years, necessitating the replacement of either the pacemaker or its batteries for the patient's survival. This means that the patient will need to undergo surgery for the replacement process which can compromise the patient's life and increase the probability of being infected, not to mention the operation cost. To overcome this problem, energy harvesters can be a safer substitute for these traditional batteries since they can convert different forms of energy into electric energy, which can be stored and used when needed. In this paper, a 2-degree-of-freedom (DOF) piezoelectric energy harvester from blood flow is designed and modeled. The harvester is designed as a cut-out beam that is fixed on the pacemaker lead that passes through the Superior Vena Cava (SVC). To protect the harvester from being highly distorted by the blood flow, a plastic barrier is added in front of the harvester from the vein's inlet side. The harvester consists of three layers, a PZT-5A layer sandwiched between two plastic layers. The harvester is designed to have its first and second natural frequencies between $1Hz$ and $1.67Hz$, the normal frequency range of the human heartbeat. The harvester harvests up to $3.8V$ which is considered satisfying since the pacemaker usually stimulates the heart using a voltage that ranges from $1V$ to $10V$. This voltage can be used to power the pacemaker and extend its lifetime. The harvester was simulated using ANSYS Workbench Software 2020 R2. On the simulation level, the harvester obtained a maximum output power of $0.81\mu W$ at a load of $2.2M\Omega$.**

***Keywords*—Finite Element Analysis; Fluid-Solid Interaction; Piezoelectric; Energy Harvesting; Cut-Out Configuration.**

I. INTRODUCTION

It is estimated that each year 1.25 million permanent pacemakers are implanted worldwide. In 2016, approximately 500,000 permanent pacemakers were implanted in Europe [1]. The pacemaker is an electronic device that is used to treat many heart rhythm conditions like bradycardia, atrial fibrillation, and heart failure. It is implanted under the skin in the chest or abdomen with leads extending to the sinus of the heart chambers through the SVC. The pacemakers are powered by a battery with a lifetime ranging from 5 to 10 years, depending on the pacemaker's activity and heart condition [2], [3]. The implanted pacemaker usually needs to be replaced with a new one during the patient's life, which may raise many risks such as infection, wound discomfort, and bruising [4]. Also, this will cost more money and time and the used chemical batteries can cause harm to the environment. To overcome these risks, scientists tried to develop devices with energy harvesting systems to increase the pacemaker's lifetime. Since then, devices have been powered by batteries, energy harvesters, or both [5], [6].

To scavenge energy from the human body, some concepts are presented including - but not limited to - electromagnetic, thermoelectric, piezoelectric, and solar cells.

A. Electromagnetic Concept

Electromagnetic energy harvesting works based on Faraday's law of electromagnetic induction [7]. A. Zurbuchen et al. [8] fixed a spring-mass system on the heart so they could use its beating vibrations to oscillate the mass. The mass motion deforms the spring, which rotates a micro-generator that generates about $80 - 90\mu W$. S. H. Kim et al. [9] developed a tiny rotor with magnets inside coils, including ferrite cores, to harvest energy from blood flow. This generator harvested about $3.4mW$. Pfenniger et al. [10] also used a miniature turbine generator, which obtained 1 mW. In another work, Pfenniger et al. [11] used the principle of translating an induction coil in a magnetic field by winding a coil around an artery, where the coil expands with the artery's expansion. This method harvested about $42nW$. Chengbo Hu et al. [12] proposed a compact magnetic levitation energy harvester with a tunable natural frequency. This harvester achieved an output power of $462.1\mu W$ at a low frequency of $9.6Hz$. Zhang et al. [13] designed an electromagnetic harvester that utilized ankle

acceleration. The harvester generated $0.5mW$ while walking at a speed of $4km/h$. Zhou et al. [14] designed an improved electromagnetic energy harvester from limb motion. Cai et al. [15] presented an enhanced electromagnetic energy harvester to be used with wrist-worn devices and harvests energy from human motion. Zhao et al. [16] designed an electromagnetic energy harvester that operates at low frequencies and irregular human motion. Maharjan et al. [17] proposed a wearable electromagnetic energy harvester that utilizes human motion to power smart wearables and monitoring devices.

B. Thermoelectric Concept

The thermoelectric concept is applied in applications where there is thermal energy that can then be converted to electric energy via the seebeck effect [18], [19]. To harvest energy via this concept, semiconductor thermocouples can be connected in series or in parallel to form a thermoelectric generator (TEG). Furthermore, to increase the output power, many sets of thermocouples can be connected to form a thermopile [20], [21]. Ren et al. [22] designed a wearable, stretchable, recyclable TEG that could generate up to $1V/cm^2$. Yang et al. [23] designed a stretchable TEG to harvest energy from the human body heat, which resulted in an output power of about $0.15mW/cm^2$.

C. Piezoelectric Concept

The piezoelectric concept is applied by several means in a huge number of applications as in sensors, microelectromechanical systems, microfluidics, etc. [24]–[29]. Abdelmageed et al. [30] designed a piezoelectric energy harvester to be placed inside the SVC and harvests energy from pulsatile blood flow to power the pacemaker. The harvested power was equal to $52nW$ at a load of $45M\Omega$. Xu et al. [31] designed a piezoelectric nanogenerator to be attached to the lead of a pacemaker and harvest energy from the lead movement. They managed to get an output energy of $6.5\mu J$. Azimi et al. [32] implanted a piezoelectric energy harvester in a large animal, obtaining an output energy of $0.487\mu J$. Bingwei et al. [33] developed a Lead Zirconate Titanate (PZT) spring to be attached to the heart, which resulted in an output voltage of about $1.5V$. Zhang et al. [34] used a flexible Polyvinylidene fluoride (PVDF) film around the aorta to make use of the internal pressure, which induced stresses in the PVDF film and subsequently generated an output power of $681nW$. Li et al. [35] implanted a piezoelectric energy harvester in an adult Yorkshire swine to directly power a pacemaker, which resulted in an output current of $15\mu A$. Mahmoud et al. [36] designed a micro-scale 2-DOF energy harvesting device that works under low-frequency conditions. The harvester utilized human motion to generate energy over a wide bandwidth of $1-10Hz$. Qian et al. [37] obtained an output power of $9mW$ by embedding a piezoelectric energy harvester into a boot and using a single-stage force amplifier. They also applied the same concept with a two-stage force amplifier, which resulted in an average output power of $34mW$ [38]. Using a parallel link topology, Asano et al. [39] incorporated six multi-layered piezoelectric stack transducers into a sole to produce an average power of $1.3mW$ from human stepping. Wen et al. [40] utilized mechanical energy from human footsteps on a two-directional piezoelectric stack-based energy harvester, which generated an average power of $7-15\mu W$ at an input force of $5.1N$. Gao et al. [41] designed a Macro-Fiber Composite (MFC) piezoelectric energy harvester from knee motion, which resulted in an average power of $1.6mW$ at a speed of $4km/h$. Wang et al. [42] proposed a piezoelectric energy harvester from human breathing to monitor the respiratory system. L. Dong et al. [43] proposed a helical-shaped piezoelectric energy harvester attached to a pacemaker lead to convert cardiac motion into electrical energy. When tested on a porcine, This resulted in an output open-circuit peak-to-peak voltage of $0.6V$ and $0.05V$ for bending motion and vibration of the lead, respectively. Naik et al. [44] proposed a piezoelectric energy harvester embedded in the shoes, which resulted in an output voltage of $3.2V$ through foot tapping. Beyaz et al. [45] proposed a piezoelectric energy harvester from waist movement. The generated open-circuit voltage ranged from $1.5V$ to $1.8V$ for normal and fast respiration processes. Ryu et al. [46] proposed harvesting energy from talking and saliva swallowing. The harvester generated an output voltage of $20mV$ for the first method and $15mV$ for the second method. Hajra et al. [47] proposed a flexible harvester that could harvest energy from clapping, exercising, and palm and finger tapping, which resulted in $(4.9V; 19.3nA)$, $(3.8V; 10nA)$, $(5.8V; 25nA)$ and $(3.2V; 17nA)$, respectively. Zhou et al. [48] developed an energy harvester from walking, which generated an output voltage of $6V$ and had a power density of up to $1.4\mu W/cm^2$. Yin et al. [49] proposed a piezoelectric energy harvester shoe that utilized the frequency up-conversion concept to harvest energy from walking.

D. Pyroelectric Concept

There is a subclass of piezoelectric materials known as the pyroelectric materials. These materials change their polarization in response to a constant temperature change [50], [51]. Mahanty et al. [52] designed a pyroelectric harvester that could obtain an energy density of $34\mu W.cm^{-2}$. Li et al. [53] designed a harvester that combined pyroelectric, solar, and thermal interfaces, which resulted in an energy density of $21.3mW.m^{-2}$.

E. Triboelectric Concept

Triboelectricity is like piezoelectricity but depends on friction instead of deformation. It is possible to harvest energy by combining both concepts as in [54]–[57]. H. Ouyang et al. [58] proposed a symbiotic cardiac pacemaker that utilized energy

harvested from cardiac motion by a triboelectric nanogenerator. The resulting output energy was equal to $0.495\mu J$.

F. Solar Concept

Solar energy can be converted into electric energy by the photovoltaic effect [59]. A. Haeberlin et al. [60] developed a pacemaker powered by solar cells. It was tested in a pig in direct sunlight, shadow, and indoors. The solar cells obtained an output power of $1963\mu W/cm^2$, $206\mu W/cm^2$, and $4\mu W/cm^2$, respectively. Bereuter et al. [61] tested the pacemaker with the solar cell system on volunteers, resulting in an output power of $67\mu W$ recorded over a year.

The previous studies can be divided into two categories: 1) External power sources such as solar energy, and 2) Mechanical energy generated from some internal organs such as the heart and arteries. The drawback of solar energy is that it works only during daytime. The second category is widely used, as in [5], [62]–[66], since it depends on the movement of human body parts and organs such as the eyelid, hands, limbs, and abdomen, etc. [67]–[70]. Also, Several studies have shown how promising biomechanical energy harvesting methods can be [71], [72].

Usually, the harvester is designed to work at a single frequency, which means that it does not take into consideration the frequency ranges of the organs. For example, the heartbeat frequency has a range of $60 - 100 beats per minute (bpm)$, i.e. $1 - 1.67Hz$.

In this paper, a study of a 2-DOF energy harvester from blood flow inside the SVC is presented. The choice of the SVC drew inspiration from the fact that the pacemaker leads usually pass through it, so the implantation process of the harvester will not require extra surgery. The study includes the selection procedure of the harvester parameters, modeling, and simulation of the harvesting system.

II. Harvester Model

The proposed harvester is a 2-DOF harvester designed based on the cut-out beam configuration shown in Fig. 1. In this configuration, there are two masses, the primary mass (m_1) and the secondary mass (m_2). Also, there are two beams, the primary and secondary beams. The primary beam is divided into two halves, and each half has a stiffness $k_1/2$, while the secondary beam is cut into the primary beam and has a stiffness k_2. The cut-out configuration is chosen over other configurations because it provides a compact design and can easily fit inside the SVC without needing extra space, unlike the L-shaped configuration and other configurations that may need to be relatively long to be able to properly operate at low frequencies. The 2-DOF is preferred over the Single-Degree-of-Freedom (SDOF) since it can capture the frequency spectrum of human heartbeat instead of just considering a single frequency. For the harvester to operate effectively within the human heartbeat frequency range ($60-100bpm$), the harvester's natural frequencies must lie within this range so it can achieve the highest deformations and hence the highest output voltage. The harvester's design approach draws inspiration from the PVDF vibration sensor (LDT0-028K). This sensor consists of three layers, a PVDF film sandwiched between two layers of plastic (MYLAR). In the proposed harvester, we have a PZT-5A layer sandwiched between two plastic (PET) layers. The reason for using these plastic layers is to isolate the harvester from the surrounding fluid domain and give it protection and flexibility. The PZT-5A material is chosen over PVDF since it has a higher piezoelectric coefficient, which results in a significantly higher generated voltage for the same applied stress. This will make the harvester more efficient for this application because the blood flow tends to be slow and cannot cause high stress. The PET material has been selected for its resilience and biocompatibility.

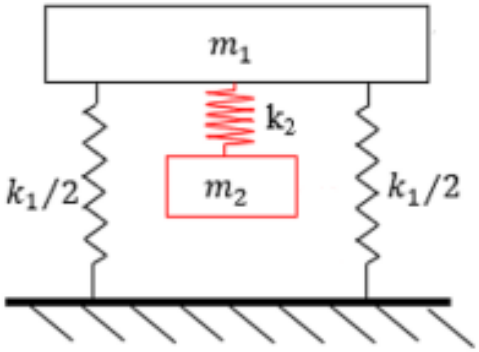

Fig. 1. Schematic Diagram for the Cut-Out Beam Configuration [74]

III. Harvester Design Procedure

This section presents the selection process for the harvester parameters based on the human heartbeat frequency range. Since the harvester is to be placed inside the SVC, its dimensions must be carefully chosen to avoid causing any blockage to the blood flow. The harvester is secured to the pacemaker lead, allowing them to be implanted in a single surgery instead of separate surgeries. Abdelmageed et al. [75] proposed and applied this concept to an SDOF harvester. The SVC has a canonical shape with a diameter that ranges from $18mm$ at the inlet to $22mm$ at the outlet [76], [77]. To select the harvester dimensions properly making sure that it will not cause blockage to the blood flow, a catheter that passes through the SVC is taken as a reference. This catheter is the hemodialysis catheter which is a permanent catheter with a diameter ranging from $d_{min} = 5.1mm$ to $d_{max} = 5.3mm$ [78], [79]. This is equivalent to a maximum cross-section area of $A_{Catheter} = \pi * (d_{max}/2)^2$ resulting in a total blockage of about $22.06mm^2$. So, the cross-section area of the harvester

and the pacemaker lead shouldn't exceed this value to avoid blood flow blockage by the harvester-lead system. The smallest pacemaker lead diameter equals $1.4mm$ [80], considering the triple-chambered pacemaker, which is equivalent to a cross-section area of $A_{Lead} = 3 * \pi * (d_{Lead}/2)^2 = 4.6mm^2$. Based on the previous calculations, the allowable cross-section area for the harvester equals $17.4mm^2$.

A study was conducted to determine the effect of different parameters on the natural frequencies of a cantilever beam. Initially, an SDOF cantilever beam was built in ANSYS using the following preliminary selected parameters: $8.5mm * 0.9mm * (0.052mm, 0.028mm, 0.125mm)$. The last three dimensions are equal to the thicknesses of the three layers of the sensor. The length of $8.5mm$ was chosen as the maximum allowable length for the harvester, assuming that the harvester is to be placed in the middle of the SVC.

As shown in Fig. 2, changing the Length from $8.5mm$ to $2mm$ led to a significant drop in the beam's natural frequency. In Fig. 3, the width was changed from $0.9mm$ to $0.5mm$ resulting in a slightly increasing natural frequency. In Fig. 4, one Mylar layer thickness was changed gradually from $0.125mm$ to $0.0025mm$ leading to a decreasing natural frequency.

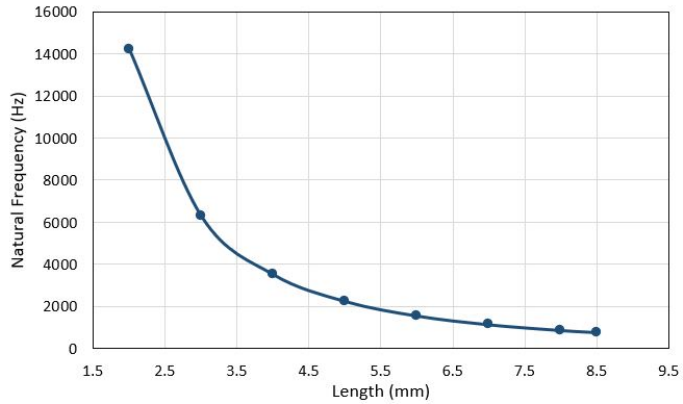

Fig. 2. Resonance Variation with Beam Length

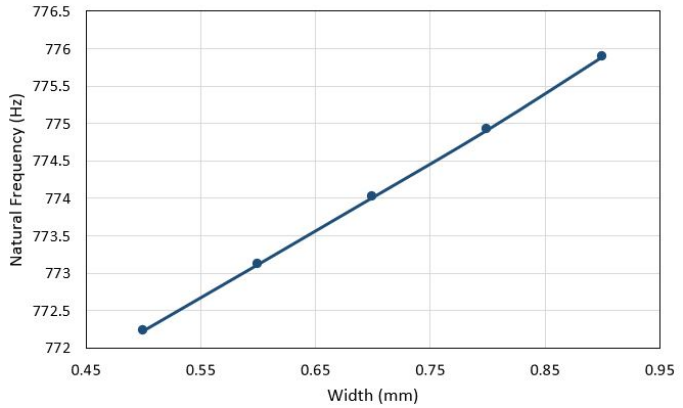

Fig. 3. Resonance Variation with Beam width

Based on the previous analysis, the dimensions of the 2-DoF harvester are $8.5mm * 2mm * (0.005mm, 0.0025mm, 0.005mm)$. According to Zayed et al. [81], The length of the secondary beam l_2 should be $l_2 \leq 2/3l_1$ for the harvester to act as a 2-DOF system not two separate SDOF beams. So, the secondary beam length is to be $5.5mm$. The $2mm$ width is divided as follows: $W_1/2 = W_2 = 0.4mm$, with the space between each two beams equal $0.4mm$ too. These dimensions still do not give the device the required natural frequencies, but they decrease its natural frequencies by a remarkable value.

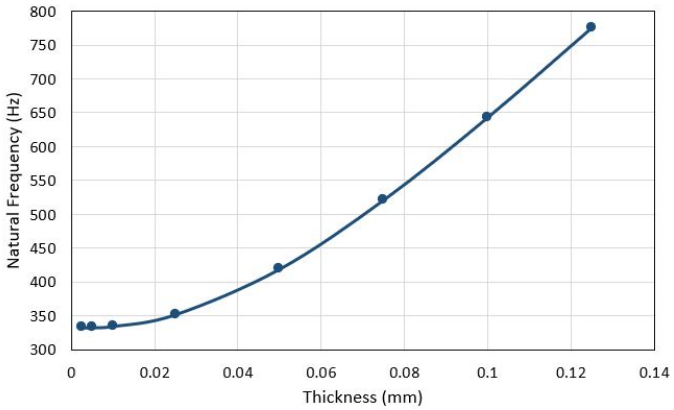

Fig. 4. Resonance Variation with Beam Thickness

To further decrease them, two methods can be considered. The first method is to add holes to the harvester's body, which will decrease the beams' stiffness and hence reduce the natural frequencies. This method is not recommended in our case since adding holes increases the harvester's weakness and still cannot provide very low natural frequencies. Since the mass is inversely proportional to the natural frequency of a beam, the second method is to add tip masses. The tip masses were tuned and added as distributed masses on the beams' tips. The values of the masses are equal to $6.2 * 10^{-5}kg$ and $3.4 * 10^{-5}kg$ for the primary and the secondary beams, respectively. The cross-section area of the harvester is equal to $9.9548 * 10^{-6}mm^2$, shown in Fig. 5.

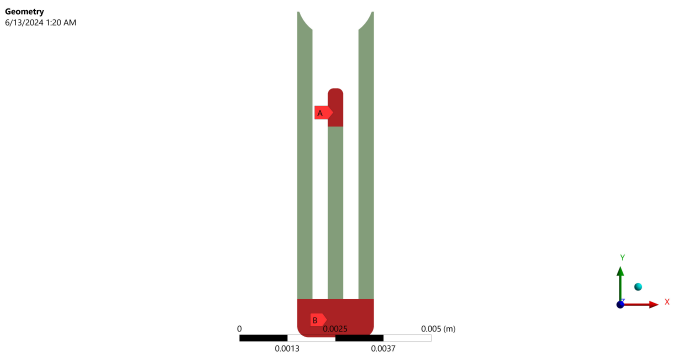

Fig. 5. Two Degrees of Freedom Harvester Model

Table I shows the parameters of the harvester obtained from this study. It lists the thicknesses of the PET and PZT layers, the lengths and widths of the primary and secondary beams, the space between the primary and secondary beams, and the tip masses of the primary and secondary beams. Fig. 6 illustrates the design procedure of the energy harvester. It outlines the simulation process using ANSYS Workbench, which includes modal analysis to study the harvester's natural frequencies, blood flow modeling, mechanical part modeling of the pacemaker lead, the barrier, and the harvester, and harmonic analysis to calculate the harvester's output voltage.

TABLE I. THE HARVESTER'S PARAMETERS

Parameter	Value
PET Layer Thickness	0.005 mm
PZT Layer Thickness	0.0025 mm
Primary Beam Length(L_1)	8.5 mm
Secondary Beam Length(L_2)	5.5 mm
Primary Beam Width($W_1/2$)	0.4 mm
Secondary Beam Width(W_2)	0.4 mm
Space between the Primary and the Secondary Beams	0.4 mm
Primary Mass(m_1)	$6.2 * 10^{-5} kg$
Secondary Mass(m_2)	$3.4 * 10^{-5} kg$

IV. SIMULATION

In this section, a simulation using ANSYS Workbench is carried out to investigate the performance of the harvester with the selected parameters. The simulation process is divided into the following parts:

- Modal Analysis: to study the harvester's natural frequencies.
- Blood Flow Modeling: to model the fluid part.
- Mechanical part Modeling: to model the Pacemaker Lead, the Barrier, and the harvester.
- Harmonic Analysis: to calculate the output voltage of the harvester.

A. Modal Analysis

In this part, the design process of a 2-DoF harvester, with its two natural frequencies tuned to be between $1Hz$ and $1.67Hz$, is explained. The harvester should be able to generate reasonable energy along this frequency range. So, it should have its first natural frequency close to $1.1Hz$ and its second natural frequency close to $1.6Hz$ to work effectively. The beams' dimensions were chosen based on the analysis done in the previous section. Then a mesh sensitivity analysis was performed to select the most suitable mesh element size. The mesh size was changed from $0.05mm$ to $0.5mm$. Element sizes above $0.2mm$ failed to generate any result, and there was no abrupt change in the frequencies with the element sizes less than or equal to $0.2mm$. To overcome this issue, we had to consider other factors such as the elements' Skewness and Aspect ratio. After studying these factors, an element size of $0.06mm$ was chosen and the capture curvature feature was activated resulting in a skewness of 0.76 and an aspect ratio of about 42. These values were considered acceptable since they provide a reasonable calculation time. The natural frequencies of the harvester at this stage were equal to $25.72Hz$ and $55.3878Hz$.

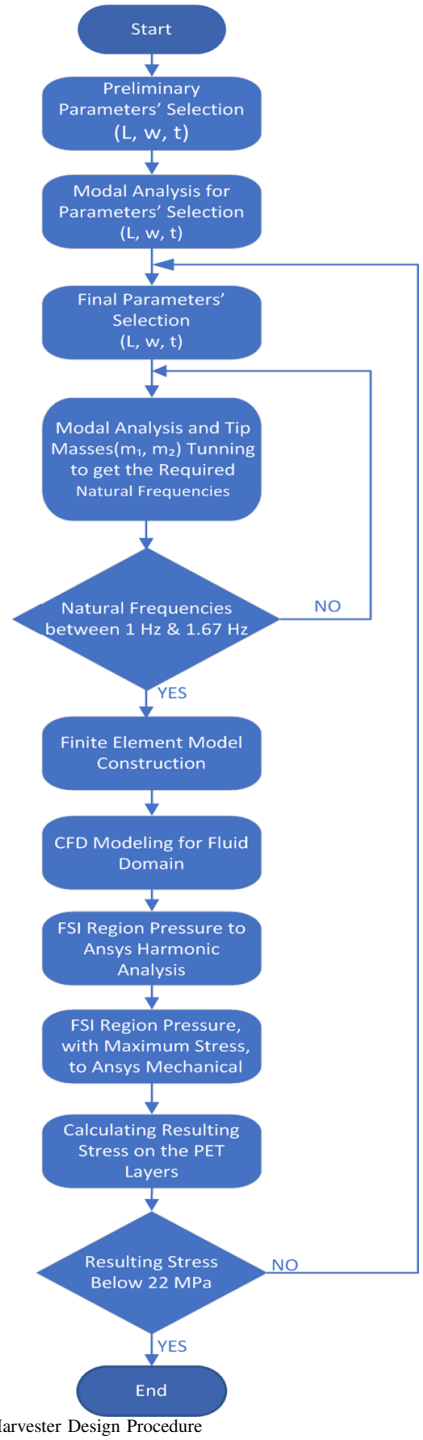

Fig. 6. Energy Harvester Design Procedure

The next step was to tune the tip masses to make the above values drop to the desired frequency values of about $1.1Hz$ and $1.6Hz$. The higher the masses, the lower the natural frequencies. Also, we need to make sure that the added masses do not cause excessive loading on the beams. This will be proven via the stress analysis in the mechanical part simulation IV-D. By tuning the masses, we were able to obtain a harvester with natural frequencies equal to $1.1076Hz$ and $1.5196Hz$, which are close enough to the frequencies stated earlier, as shown in Fig. 7 and Fig. 8, respectively.

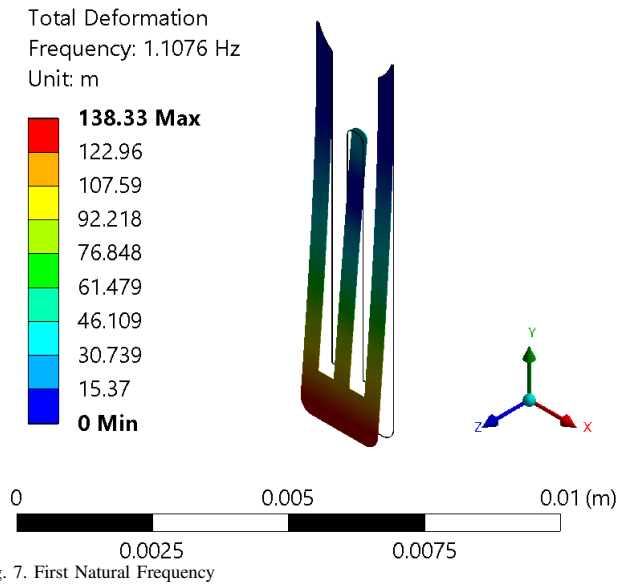

Fig. 7. First Natural Frequency

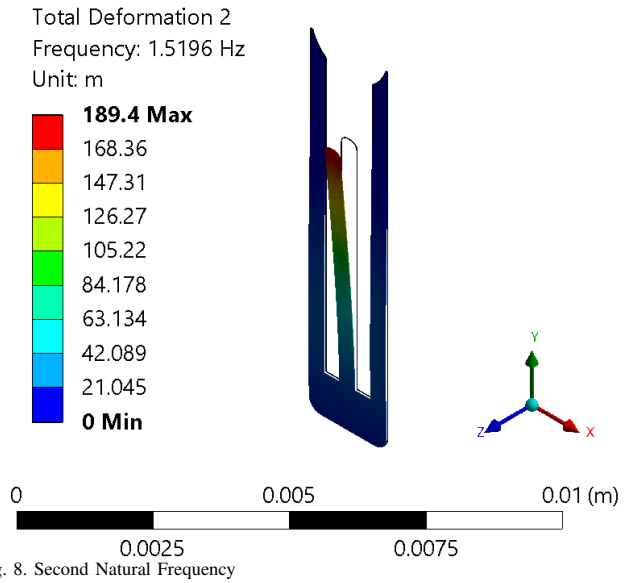

Fig. 8. Second Natural Frequency

B. Blood Flow Modeling

The fluid domain was modeled as a cone with the SVC dimensions mentioned in Section III. At first, mesh sensitivity analysis was performed to select a suitable mesh element size. The element size was changed gradually from $2mm$ to $0.2mm$, and the change in the area-weighted pressure at the Fluid-Solid Interaction (FSI) region was observed. At last, an element size of $1mm$ was chosen based on an error of 10% in the variation of the pressure with the mesh element size. The 10% error was considered acceptable to maintain reasonable calculation time. To capture the features of the region in concern, the FSI region, the capture curvature and capture proximity features were activated to provide finer mesh around this region.

To model the fluid domain, ANSYS fluent was used. In fluent, the mesh was converted to a polyhedral mesh, as shown in Fig. 9, to reduce the number of elements and improve their quality. The final number of elements was equal to 313644 elements.

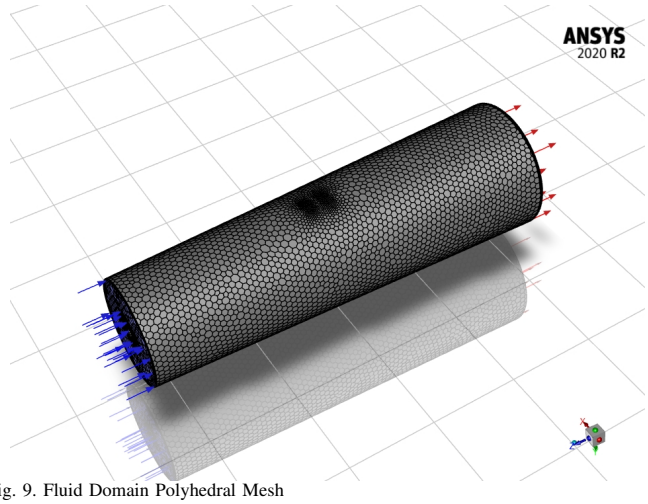

Fig. 9. Fluid Domain Polyhedral Mesh

According to Abdelmageed et al. [61], [75], the pulsatile blood flow inside the SVC can be represented by piecewise functions for the inlet velocity and the outlet pressure as follows Table II and III:

TABLE II. INLET VELOCITY PIECEWISE FUNCTION

Start	End	Function
0	0.5	$-0.5\ cos(3\pi t) + 0.5$
0.5	0.85	$-0.25\ cos(6\pi t + 0.5\pi) + 0.5$
0.85	1	$-0.5\ cos(3\pi t + \pi) + 0.5$

TABLE III. OUTLET PRESSURE PIECEWISE FUNCTION

Start	End	Function
0	0.09	$0.4\ cos(5.5\pi t) + 0.6$
0.09	0.18	$0.1\ cos(22\pi t + 0.5\pi) + 0.6$
0.18	0.5	$0.125\ cos(4.4\pi t - 22\pi/5.1) + 0.6$
0.5	0.8	$0.3246\ cos(3.52\pi t + 5.5\pi/3) + 0.4$
0.8	1	$0.45\ cos(5\pi t + 5\pi) + 0.526$

The piecewise functions result in the profiles shown in Fig. 10 and Fig. 11, for the velocity and pressure respectively.

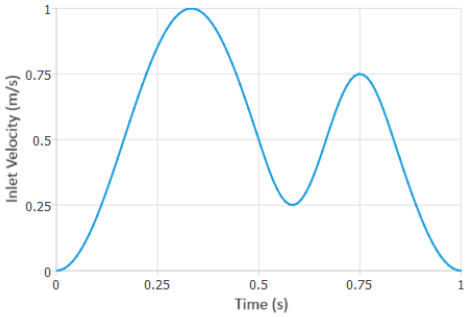

Fig. 10. Inlet Velocity Profile

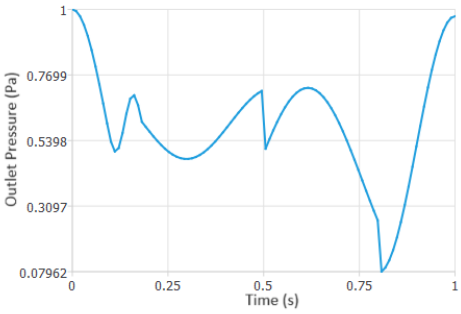

Fig. 11. Outlet Pressure Profile

The blood flow is a Transient laminar flow with the following material properties in Table IV:

TABLE IV. BLOOD PROPERTIES [82]

Property	Value
Density (kg/m^3)	1060
Viscosity $(kg/m.s)$	Carreau
Time Constant, Lambda (s)	0.3568
Zero Shear Viscosity (kg/m^3)	0.056
Infinite Shear Viscosity (kg/m^3)	0.0035

After defining the fluid and the flow properties, the equations of the flow conditions were inserted as User Defined Functions - UDFs - in fluent as follows Table V:

TABLE V. UDFS INSERTED IN ANSYS FLUENT FOR INLET VELOCITY AND OUTLET PRESSURE THROUGH THE SVC

Parameter	Function
V_1	$(-0.5 * cos(3 * PI * t/1[s]) + 0.5) * 1[m/s]$
V_2	$(-0.25 * cos(6 * PI * t/1[s] + 0.5 * PI) + 0.5) * 1[m/s]$
V_3	$(-0.5 * cos(3 * PI * t/1[s] + PI) + 0.5) * 1[m/s]$
P_1	$(0.4 * cos(5.5 * PI * t/1[s]) + 0.6) * 1[Pa]$
P_2	$(0.1 * cos(22 * PI * t/1[s] + 0.5 * PI) + 0.6) * 1[Pa]$
P_3	$(0.125 * cos(4.4 * PI * t/1[s] - 22 * PI/5.1) + 0.6) * 1[Pa]$
P_4	$(0.3246 * cos(3.52 * PI * t/1[s] + 5.5 * PI/3) + 0.4) * 1[Pa]$
P_5	$(0.45 * cos(5 * PI * t/1[s] - 5 * PI) + 0.526) * 1[Pa]$

The last step was to initialize and run the simulation. After the fluid part simulation was done in ANSYS Fluent, the pressure in the FSI region was exported into ANSYS Mechanical to determine whether the harvester is strong enough to bear this pressure. This resulted in a highly distorted structure, which means that the harvester was too weak to bear the flow pressure directly. To reduce the flow pressure on the harvester to an acceptable value, a barrier was added in front of the harvester. It was placed parallel to the harvester from the SVC inlet side. It is made of PET and has the same outer dimensions as the harvester with a thickness equal to $0.1mm$. Fig. 12 shows the generated mesh around the FSI region after adding the barrier. At last, the fluid domain was modeled, and the pressure at the FSI region at different timesteps was exported. This pressure was fed to mechanical analysis to study the deformations and stresses on the harvester.

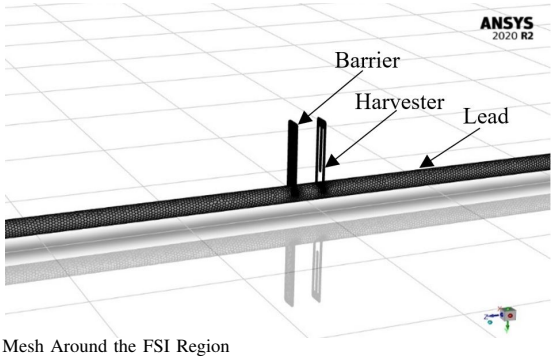

Fig. 12. Mesh Around the FSI Region

Fluent simulation was run with a step size of $0.01s$ for the $1second$ duration of one cycle of the flow, and the pressure on the FSI region was exported each $0.05s$ and fed into mechanical and harmonic analysis. Fig. 13, Fig. 14, Fig. 15 and Fig. 16 show how the velocity and pressure contours look like at different timesteps.

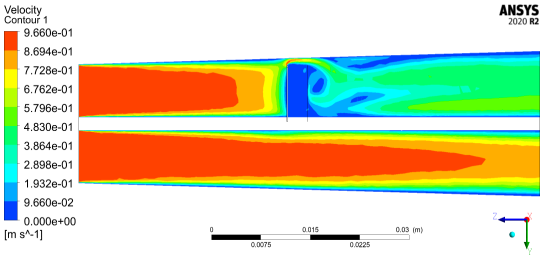

Fig. 13. Velocity Contour at 0.4s

C. Harmonic Analysis

In this part, the pressure induced on the FSI zone due to the fluid flow was exported every $0.05s$. This pressure was fed into the harmonic analysis to calculate the respective stresses and voltages on a frequency range of $0.1 - 2Hz$. The process of calculating the voltage frequency response in ANSYS takes too much time. To reduce the calculation time, the stress was calculated and plotted at each pressure and then the stress

values at both natural frequencies were plotted versus time for a duration of $1s$, which is the time of one flow cycle.

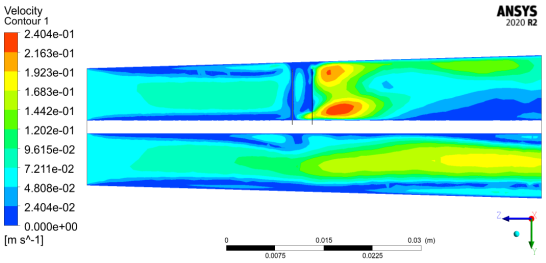

Fig. 14. Velocity Contour at 0.95s

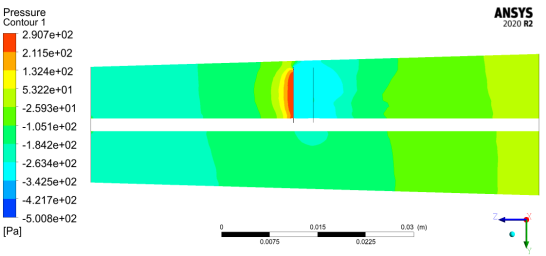

Fig. 15. Pressure Contour at 0.4s

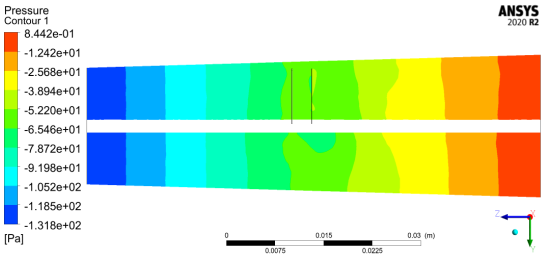

Fig. 16. Pressure Contour at 0.95s

For piezoelectric materials, the output voltage value depends on the stress applied on the piezoelectric beam. So, the stress-time plots shown in Fig. 17 can be used as a reference for how the voltage profile will look like at each natural frequency during the $1s$ duration. As illustrated below in Fig. 17 the stress is maximum at $0.95s$ and $0.4s$ at the first and the second natural frequencies, respectively.

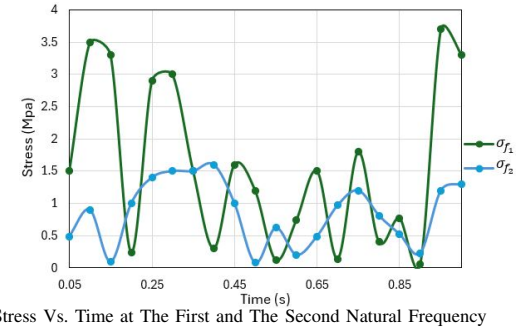

Fig. 17. Stress Vs. Time at The First and The Second Natural Frequency

D. Mechanical Part Modeling

In this part, the flow pressure, at $0.95s$ and $0.4s$, that caused the highest stress at the beams' natural frequencies at the FSI region according to the harmonic analysis, was fed into ANSYS structural analysis to make sure that the resulting stresses on the harvester are within the allowable limits for the lead beam, i.e. the PET layers. The simulation was run with $0.01s$ timestep size. The large deflection feature was activated, and the Direct solver was chosen as it can handle nonlinear solutions, i.e. large deformations, better. The resulting defections at $0.4s$ and $0.95s$ are shown in Fig. 18 and Fig. 20, respectively. Also, It was found that the equivalent von mises stress is equal to $14MPa$ at $0.4s$ and $20MPa$ at $0.95s$ as shown in Fig. 19 and Fig. 21, respectively. According to [83], these values are less than the maximum allowable stress for the PET material which has a lower limit of $22MPa$.

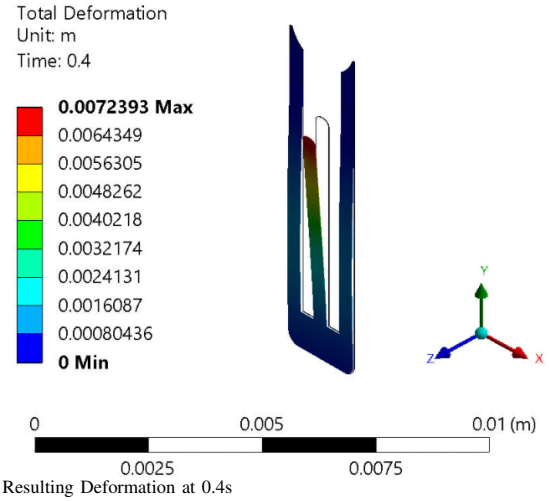

Fig. 18. Resulting Deformation at 0.4s

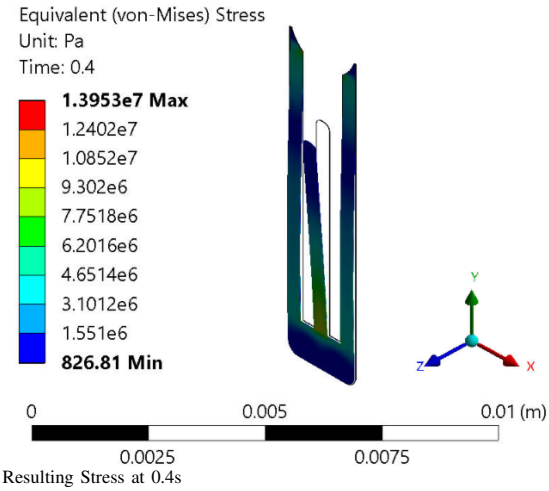

Fig. 19. Resulting Stress at 0.4s

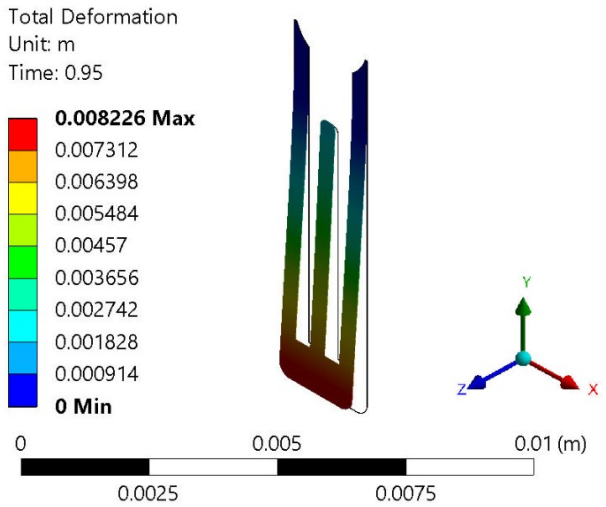

Fig. 20. Resulting Deformation at 0.95s

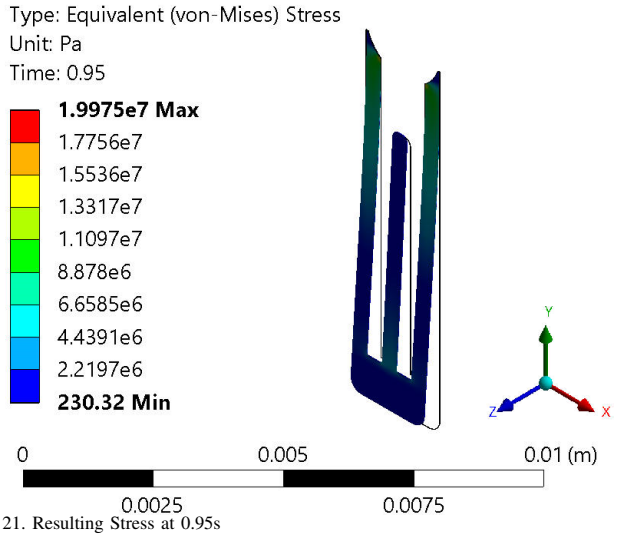

Fig. 21. Resulting Stress at 0.95s

V. Results and Discussion

In this section, the results of the simulation process are presented and discussed. As concluded from the previous section, the maximum stress occurred at $0.95s$ and $0.4s$ for the first and the second natural frequencies, respectively. This resulted in maximum voltage generation at these timesteps. Fig. 22 shows that the maximum voltage generated are $V_{max}^{f_1,0.95s}$=3.8V, and $V_{max}^{f_2,0.4s}$=0.7V at the corresponding natural frequencies. The natural frequencies extracted from harmonic analysis are f_1=1.1287 Hz and f_2=1.5484 Hz, which are close to the frequencies calculated by modal analysis of $1.1076Hz$ and $1.5196Hz$. This difference will not affect the harvester's performance since the obtained frequencies are still very close to the boundaries that were set at the beginning, which are $f_1 = 1.1Hz$ and $f_2 = 1.6Hz$.

This difference can be caused by the fact that modal analysis calculates the natural frequencies based on the structure's mechanical properties, unlike harmonic analysis which considers external loads in the form of periodic functions, making a forced response. Also, this analysis is very sensitive to the loading condition, and therefore the response of the structure at different excitation frequencies, more so near the natural frequencies, can vary by orders of magnitude. The generated voltage values change depending on the stress applied as mentioned in Section IV-C. For example, at $1s$, V_{f_1}=3.38V, V_{f_2}=0.63V.

The following equations can be used to calculate the power generated by the harvester [74], [84], [85]:

$$C = \frac{K^T \epsilon_0 A}{t} \tag{1}$$

$$Z_p = \frac{1}{2\pi f C} \tag{2}$$

$$V_l = \frac{V_{oc} R_l}{|Z_p + R_l|} \tag{3}$$

$$P_l = \frac{|V_{oc}|^2 R_l}{2|Z_p + R_l|^2} \tag{4}$$

Where C is the Capacitance of the Piezo Element, K^T is the Relative Dielectric Constant ($K^T = 1800$), ϵ_0 is the Permittivity of Free Space ($\epsilon_0 = 8.854 * 10^{-12} F/m$), A is the Surface Area of the Piezo Element ($A = 9.9548 * 10^{-6} m$), t is the Thickness of the Piezo Element ($t = 0.0025 * 10^{-3} m$), Z_p is the Piezoelectric Impedance, f is the Operating Frequency, V_oc is the Open Circuit Voltage generated by the Piezo Element, R_l is the Impedance of the load connected to the harvester, V_l is the Output (Load) Voltage and P_l is the Output (Load) Power. The output power and voltage were calculated over two different ranges for the load impedance.

The first range is from $100K\Omega$ to $1G\Omega$ as shown in Fig. 23 and Fig. 24, while the second range is associated with the pacemaker impedance, shown in Fig. 25 and Fig. 26, and ranges from 500Ω to 900Ω as mentioned in the pacemaker datasheet provided by Medtronic [86].

Table VI shows the maximum load Voltage and load power over both ranges at the first and second natural frequencies of the harvester.

TABLE VI. Maximum Load Voltage and Power over Both Ranges

Impedance Range	Parameter	Value	R_l
$100K\Omega$ to $1G\Omega$	$V_l^{f_1}$	3.7916V	$1G\Omega$
	$V_l^{f_2}$	0.6989V	$1G\Omega$
	$P_l^{f_1}$	0.81μW	2.2$M\Omega$
	$P_l^{f_2}$	37.82nW	1.6$M\Omega$
500Ω to 900Ω	$V_l^{f_1}$	0.0015V	900Ω
	$V_l^{f_2}$	0.39mV	900Ω
	$P_l^{f_1}$	1.3nW	900Ω
	$P_l^{f_2}$	0.084nW	900Ω

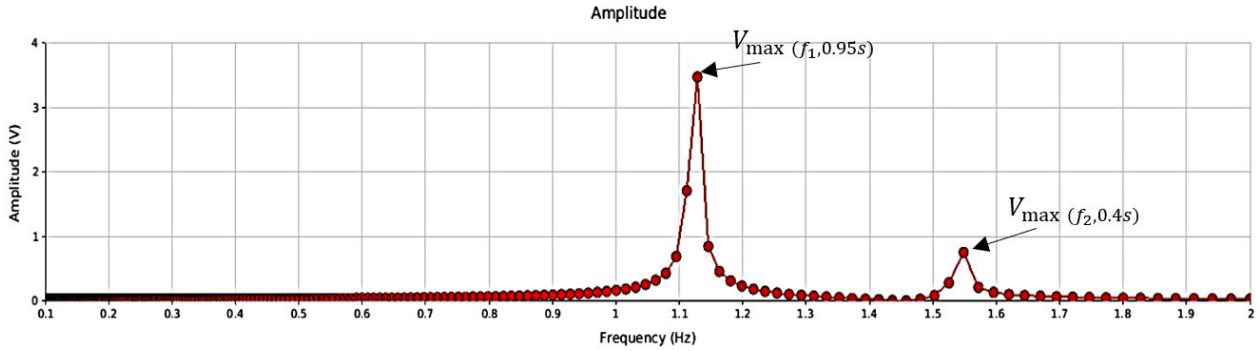

Fig. 22. Maximum Voltage Generated by The Harvester

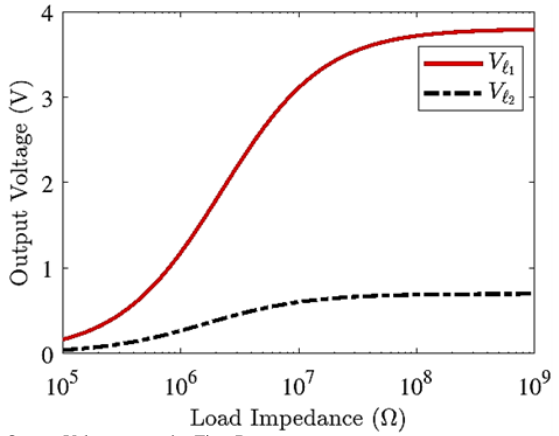

Fig. 23. Output Voltage over the First Range

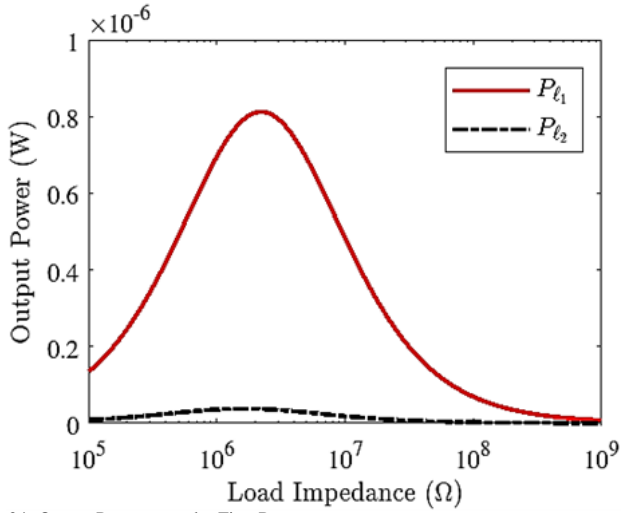

Fig. 24. Output Power over the First Range

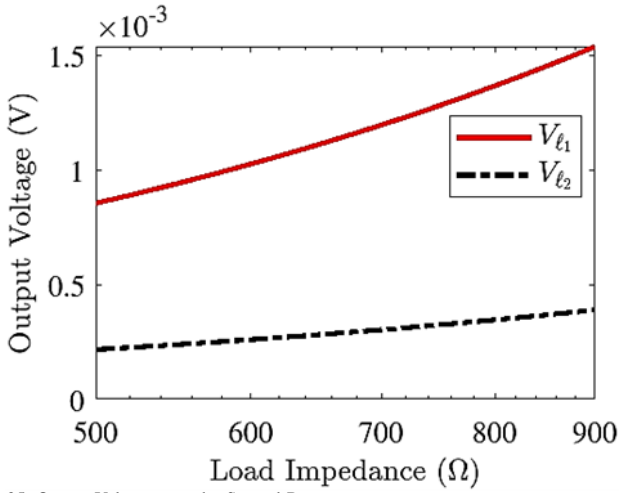

Fig. 25. Output Voltage over the Second Range

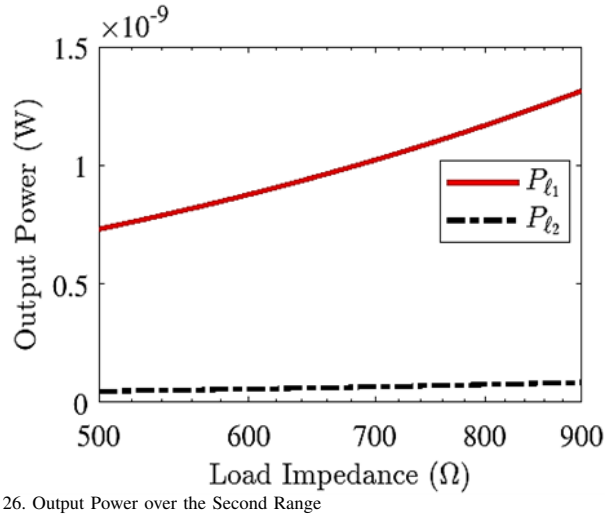

Fig. 26. Output Power over the Second Range

Table VII presents a comparative analysis of the energy harvesters in previous studies and the proposed harvester. The comparison was done based on the harvesting concept, implantation region, harvested power, and whether or not the implantation process requires a separate surgery.

The pacemaker requires energy of about $15\mu J$ [87], and the maximum power that can be generated by the harvester is equal to $0.81\mu J/s$. This will take the harvester about $\frac{15}{0.81} = 18.5s$ to generate the energy required to power the pacemaker. On

the other hand, the $0.81\mu J/s$ will increase the lifespan of the pacemaker by about $\frac{0.81 * 100\%}{15} = 5.4\%$.

TABLE VII. COMPARISON BETWEEN THE PROPOSED HARVESTER AND THE HARVESTERS IN LITERATURE

Concept/ Source	Author	Generated Power	Implantation Region	S.S.[1]
Mechanical Energy	Zurbuchen et al. [8]	$80 - 90\mu W$	outer heart surface	Yes
Electromagnet	Pfenniger et al. [10]	$1mW$	internal thoracic artery	Yes
Piezoelectric	Bingwei et al. [33]	$1.5V$	outer heart surface	Yes
Piezoelectric	Zhang et al. [34]	$681nW$	ascending aorta	Yes
Solar Energy	Bereuter et al. [61]	$67\mu W$	arm	Yes
Piezoelectric/ Blood Flow	Proposed Harvester	$0.81\mu W$ at $2.2M\Omega$, $1.3nW$ at 900Ω	superior vena cava	No

Though the harvester did not obtain the maximum power, the concept is simple and doesn't need extra surgery for implementation. Furthermore, the proposed harvester has a very small thickness, which makes it easier to deform and hence more sensitive to the blood flow conditions. Also, the generated power can be enhanced by studying the integration of multiple harvesters on the lead. Though the harvesters in the literature provide higher output power, they do not take into consideration the frequency spectrum of the human heartbeat. Also, as mentioned before, they need a separate surgery to be implanted inside the human body.

VI. CONCLUSION

In this paper, a 2-DOF Piezoelectric energy harvester from blood flow using the PVDF vibration sensor design and the cut-out beam configuration was designed to power implanted devices, most specifically pacemakers, instead of traditional chemical batteries. The Harvester was modeled using ANSYS software. The proposed arrangement consists of the pacemaker lead with the harvester fixed on it. This arrangement is placed inside the SVC with the hemodialysis catheter taken as a reference for determining the limitations on the proposed system's dimensions. A plastic barrier was placed in front of the harvester to reduce the flow pressure on the harvester. The proposed harvester has a total area of $9.9548 * 10^{-6} mm^2$. The catheter's cross-section area is equal to $22.06mm^2$, and the barrier-lead cross-section area is equal to $19.1789mm^2$. The simulation resulted in a generated voltage of $V_{max}^{f_1,0.95s} 3.8Volts$, and $V_{max}^{f_2,0.4s}$=$0.7Volt$. Also, the maximum output power obtained is equal to $P_l^{f_1,2.2M\Omega}$=$0.81\mu W$.

VII. FUTURE WORK

- A micro-scale harvester with the same design should be tested in an artificial test rig that has the same conditions as the SVC.
- The design can be optimized to generate higher voltage to power more than one device.
- A study on multiple harvesters distributed on the pacemaker lead can be performed to generate higher voltage.
- In the proposed model, the vein and the pacemaker lead were assumed to be fixed, which is not the real case. So, as an improvement, the stability and movement conditions of the vein and the pacemaker lead can be taken into consideration for more realistic modeling of the system.
- The flexibility of the lead and the harvester materials can be studied to optimize materials selection and, consequently, enhance the output.

REFERENCES

[1] M. J. P. Raatikainen, "A decade of information on the use of cardiac implantable electronic devices and interventional electrophysiological procedures in the European Society of Cardiology Countries: 2017 report from the European Heart Rhythm Association," *EP Europace*, vol. 19, no. 2, 2017, doi: 10.1093/europace/eux258.

[2] F. Kusumoto *et al*., *Cardiac Pacing for the Clinician,* Springer Science & Business Media, 2008.

[3] V. S. Mallela, V. Ilankumaran, and N. S. Rao, "Trends in cardiac pacemaker batteries," *Indian Pacing and Electrophysiology Journal,* vol. 4, no. 4, pp. 201–2012, 2004.

[4] F. M. U. Md, "Pacemaker Generator Replacement Information for Patients," *Herz*, vol. 44, 2019, doi: 10.1007/s00059-017-4658-y.

[5] Y. Song, D. Mukasa, H. Zhang, and W. Gao, "Self-powered wearable biosensors," *Accounts of Materials Research*, vol. 2, no. 3, pp. 184-197, 2021, doi: 10.1021/accountsmr.1c00002.

[6] P. Tan, Y. Zou, Y. Fan, and Z. Li, "Self-powered wearable electronics," *Wearable Technologies*, vol. 1, 2020, doi: 10.1017/wtc.2020.3.

[7] M. Liu, F. Qian, J. Mi, and L. Zou, "Biomechanical energy harvesting for wearable and mobile devices: State-of-the-art and future directions," *Applied Energy*, vol. 321, 2022, doi: 10.1016/j.apenergy.2022.119379.

[8] A. Zurbuchen *et al*., "The Swiss approach for a heartbeat-driven lead-and batteryless pacemaker," *Heart rhythm*, vol. 14. no. 2, pp. 294-299, 2017, doi: 10.1016/j.hrthm.2016.10.016.

[9] S. H. Kim, C. -H. Yu and K. Ishiyama, "Rotary-Type Electromagnetic Power Generator Using a Cardiovascular System As a Power Source for Medical Implants," in *IEEE/ASME Transactions on Mechatronics*, vol. 21, no. 1, pp. 122-129, 2016, doi: 10.1109/TMECH.2015.2436910.

[10] A. Pfenniger *et al*., "Design and realization of an energy harvester using pulsating arterial pressure," *Medical Engineering & Physics*, vol. 35, no. 9, pp. 1256–1265, 2013, doi: 10.1016/j.medengphy.2013.01.001.

[11] A. Pfenniger, R. Volgel, V. M. Koch, and M. Jonsson, "Performance analysis of a miniature turbine generator for intracorporeal energy harvesting," *Artificial organs*, vol. 38, no. 5, pp. E68-E81, 2014, doi: 10.1111/aor.12279.

[12] C. Hu, X. Wang, Z. Wang, S. Wang, Y. Liu, Y. Li, "Electromagnetic vibrational energy harvester with targeted frequency-tuning capability based on magnetic levitation," *Nanotechnology and Precision Engineering*, vol. 7, no. 4, 2024, doi: 10.1063/10.0025788.

[13] L. B. Zhang, H. L. Dai, Y. W. Yang, and L. Wang, "Design of high-efficiency electromagnetic energy harvester based on a rolling magnet," *Energy conversion and management*, vol. 185, pp. 202-210, 2019, doi: 10.1016/j.enconman.2019.01.089.

[14] N. Zhou *et al*., "Enhanced swing electromagnetic energy harvesting from human motion," *Energy*, vol. 228, 2021, doi: 10.1016/j.energy.2021.120591.

[15] M. Caia and W. H. Liao, "Enhanced electromagnetic wrist-worn energy harvester using repulsive magnetic spring," *Mechanical Systems and Signal Processing*, vol. 150, 2021, doi: 10.1016/j.ymssp.2020.107251.

[16] L. C. Zhao *et al*., "Design, modeling and experimental investigation of a magnetically modulated rotational energy harvester for low frequency and irregular vibration," *Science China Technological Sciences*, vol. 63, pp. 2051-2062, 2020, doi: 10.1007/s11431-020-1595-x.

[17] P. Maharjan *et al*., "High-performance cycloid inspired wearable electromagnetic energy harvester for scavenging human motion energy," *Applied Energy*, vol. 256, 2019, doi: 10.1016/j.apenergy.2019.113987.

[18] Q. H. Zhang *et al*., "Thermoelectric devices for power generation: recent progress and future challenges," *Advanced engineering materials*, vol. 18, no. 2, pp. 194-213, 2016, doi: 10.1002/adem.201500333.

[19] A. R. M. Siddique, S. Mahmud, and B. V. Heyst, "A review of the state of the science on wearable thermoelectric power generators (TEGs) and their existing challenges," *Renewable and Sustainable Energy Reviews*, vol. 73, pp. 730-744, 2017, doi: 10.1016/j.rser.2017.01.177.

[20] E. W. Zaia *et al*., "Progress and perspective: soft thermoelectric materials for wearable and Internet-of-Things applications," *Advanced Electronic Materials*, vol. 5, no. 11, 2019, doi: 10.1002/aelm.201800823.

[21] Y. Wang *et al*., "Flexible thermoelectric materials and generators: challenges and innovations," *Advanced Materials*, vol. 31, no. 29, 2019, doi: 10.1002/adma.201807916.

[22] W. Ren *et al*., "High-performance wearable thermoelectric generator with self-healing, recycling, and Lego-like reconfiguring capabilities," *Science advances*, vol. 7, no. 7, 2021, doi: 10.1126/sciadv.abe0586.

[23] Y. Yang *et al*., "Stretchable nanolayered thermoelectric energy harvester on complex and dynamic surfaces," *Nano letters*, vol. 20, no. 6, pp. 4445-4453, 2020, doi: 10.1021/acs.nanolett.0c01225.

[24] M. I. Beyaz, "An acoustic blood pressure sensing scheme using time of flight and shear wave elastography techniques," *Sensors and Actuators A: Physical*, vol. 330, 2021, doi: 10.1016/j.sna.2021.112865.

[25] Y. Chen *et al*., "Wearable actuators: An overview," *Textiles*, vol. 1, no. 2, pp. 283-321, 2021, doi: 10.3390/textiles1020015.

[26] S. D. Mahapatra *et al*., "Piezoelectric materials for energy harvesting and sensing applications: roadmap for future smart materials," *Advanced Science*, vol. 8, no. 17, 2021, doi: 10.1002/advs.202100864.

[27] A. Veronica and I. M. Hsing, "An insight into tunable innate piezoelectricity of silk for green bioelectronics," *ChemPhysChem*, vol. 22, no. 22, pp. 2266-2280, 2021, doi: 10.1002/cphc.202100279.

[28] M. J. Nagaraj *et al*., "Study and Optimization of Piezoelectric Materials for MEMS Biochemical Sensor Applications," in *Advances in Renewable Energy and Electric Vehicles*, vol. 767, pp. 419–425, 2021, doi: 10.1007/978-981-16-1642-6_32.

[29] D. H. Wang, Y. H. Peng, L. K. Tang, and H. Q. Yu, "A multichamber piezoelectric pump based on pumping unit with double circular piezoelectric unimorph actuators," *Smart Materials and Structures*, vol. 30, no. 9, 2021, doi: 10.1088/1361-665X/ac182d.

[30] M. G. Abdelmageed, A. M. R. Fathelbab and A. A. Abouelsoud, "Design and simulation of an energy harvester utilizes blood pressure variation inside superior vena cava," *2019 58th Annual Conference of the Society of Instrument and Control Engineers of Japan (SICE)*, pp. 1107-1112, 2019, doi: 10.23919/SICE.2019.8859911.

[31] Z. Xu *et al*., "Flexible energy harvester on a pacemaker lead using multibeam piezoelectric composite thin films," *ACS applied materials & interfaces*, vol. 12, no. 30, pp. 34170-34179, 2020, doi: 10.1021/acsami.0c07969.

[32] S. Azimi *et al*., "Self-powered cardiac pacemaker by piezoelectric polymer nanogenerator implant," *Nano Energy*, vol. 83, 2021, doi: 10.1016/j.nanoen.2021.105781.

[33] B. Lu *et al*., "Ultra-flexible piezoelectric devices integrated with heart to harvest the biomechanical energy," *Scientific reports*, vol. 5, no. 1, 2015, doi: 10.1038/srep16065.

[34] H. Zhang *et al*., "A flexible and implantable piezoelectric generator harvesting energy from the pulsation of ascending aorta: in vitro and in vivo studies," *Nano Energy*, vol. 12, pp. 296-304, 2015, doi: 10.1016/j.nanoen.2014.12.038.

[35] N. Li *et al*., "Direct powering a real cardiac pacemaker by natural energy of a heartbeat," *ACS nano*, vol. 13, no. 13, pp. 2822-2830, 2019, doi: 10.1021/acsnano.8b08567.

[36] M. M. Magdy *et al*., "Human motion spectrum-based 2-DOF energy harvesting device: Design methodology and experimental validation," *Procedia Engineering*, vol. 87, pp. 1218-1221, 2014, doi: 10.1016/j.proeng.2014.11.387.

[37] F. Qian, T. B. Xu, and L. Zuo, "Material equivalence, modeling and experimental validation of a piezoelectric boot energy harvester," *Smart Materials and Structures*, vol. 28, no. 7, 2019, doi: 10.1088/1361-665X/ab1eb7.

[38] F. Qian, T. B. Xu, and L. Zuo, "Piezoelectric energy harvesting from human walking using a two-stage amplification mechanism," *Energy*, vol. 189, 2019, doi: 10.1016/j.energy.2019.116140.

[39] S. Asano *et al*., "Energy harvester for safety shoes using parallel piezoelectric links," *Sensors and actuators a: physical*, vol. 309, 2020, doi: 10.1016/j.sna.2020.112000.

[40] S. Wen, Z. Wu and Q. Xu, "Design of a Novel Two-Directional Piezoelectric Energy Harvester With Permanent Magnets and Multistage Force Amplifier," in *IEEE Transactions on Ultrasonics, Ferroelectrics, and Frequency Control,* vol. 67, no. 4, pp. 840-849, 2020, doi: 10.1109/TUFFC.2019.2956773.

[41] F. Gao *et al*., "Macro fiber composite-based energy harvester for human knee," *Applied Physics Letters*, vol. 115, no. 3, 2019, doi: 10.1063/1.5098962.

[42] Q. Wang *et al*., "Wearable multifunctional piezoelectric MEMS device for motion monitoring, health warning, and earphone," *Nano Energy*, vol. 89, 2021, doi: 10.1016/j.nanoen.2021.106324.

[43] L. Dong *et al*., "In vivo cardiac power generation enabled by an integrated helical piezoelectric pacemaker lead," *Nano Energy*, vol. 66, 2019, doi: 10.1016/j.nanoen.2019.104085.

[44] R. Naik *et al*., "Piezoelectric property investigation on PVDF/ZrO2/ZnO nanocomposite for energy harvesting application," *Engineering Research Express*, vol. 3, no. 2, 2021, doi: 10.1088/2631-8695/abf2cc.

[45] M. I. Beyaz and N. Ahmed, "A belt-integrated piezoelectric energy harvester for wearable electronic devices," *Ferroelectrics*, vol. 585, no. 1, pp. 187-197, 2021, doi: 10.1080/00150193.2021.1991217.

[46] C. Ryu *et al*., "PVDF-bismuth titanate based self-powered flexible tactile sensor for biomechanical applications," *Materials Letters*, vol. 309, 2022, doi: 10.1016/j.matlet.2021.131308.

[47] S. Hajra *et al*., "Piezoelectric nanogenerator based on flexible PDMS–BiMgFeCeO 6 composites for sound detection and biomechanical energy harvesting," *Sustainable Energy & Fuels*, vol. 5, no. 23, pp. 6049-6058, 2021, doi: 10.1039/D1SE01587G.

[48] X. Zhou *et al*., "All 3D-printed stretchable piezoelectric nanogenerator with non-protruding kirigami structure," *Nano Energy*, vol. 72, 2020, doi: 10.1016/j.nanoen.2020.104676.

[49] Z. Yin *et al*., "A shoe-mounted frequency up-converted piezoelectric energy harvester," *Sensors and Actuators A: Physical*, vol. 318, 2021, doi: 10.1016/j.sna.2020.112530.

[50] R. A. Surmenev *et al*., "A review on piezo-and pyroelectric responses of flexible nano-and micropatterned polymer surfaces for biomedical sensing and energy harvesting applications," *Nano Energy*, vol. 79, 2021, doi: 10.1016/j.nanoen.2020.105442.

[51] I. Sobianin, S. D. Psoma, and A. Tourlidakis, "Recent advances in energy harvesting from the human body for biomedical applications," *Energies*, vol. 15, no. 21, 2022, doi: 10.3390/en15217959.

[52] B. Mahanty *et al*., "All-fiber pyro-and piezo-electric nanogenerator for IoT based self-powered health-care monitoring," *Materials Advances*, vol. 2, no. 13, pp. 4370-4379, 2021, doi: 10.1039/D1MA00131K.

[53] H. Li *et al*., "A wearable solar-thermal-pyroelectric harvester: Achieving high power output using modified rGO-PEI and polarized PVDF," *Nano Energy*, vol. 73, 2020, doi: 10.1016/j.nanoen.2020.104723.

[54] J. Zhao and Y. Shi, "Boosting the durability of triboelectric nanogenerators: a critical review and prospect," *Advanced Functional Materials*, vol. 33, no. 14, 2023, doi: 10.1002/adfm.202213407.

[55] K. Venugopal *et al*., "Comprehensive review on triboelectric nanogenerator based wrist pulse measurement: Sensor fabrication and diagnosis of arterial pressure," *ACS sensors*, vol. 6, no. 5, pp. 1681-1694, 2021, doi: 10.1021/acssensors.0c02324.

[56] F. G. Torres and G. E. De-la-torre, "Polysaccharide-based triboelectric nanogenerators: A review," *Carbohydrate Polymers*, vol. 251, 2021, doi: 10.1016/j.carbpol.2020.117055.

[57] R. Zhang and H. Olin, "Material choices for triboelectric nanogenerators: A critical review," *EcoMat*, vol. 2, no. 4, 2020, doi: 10.1002/eom2.12062.

[58] H. Ouyang *et al*., "Symbiotic cardiac pacemaker," *Nature communications*, vol. 10, no. 1, 2019, doi: 10.1038/s41467-019-09851-1.

[59] J. Zhao *et al*., "Self-Powered implantable medical devices: photovoltaic energy harvesting review," *Advanced healthcare materials*, vol. 9, no. 17, 2020, doi: 10.1002/adhm.202000779.

[60] A. Haeberlin *et al*., "The first batteryless, solar-powered cardiac pacemaker," *Heart rhythm*, vol. 12, no. 6, pp. 1317-1323, 2015, doi: 10.1016/j.hrthm.2015.02.032.

[61] L. Bereuter *et al*., "Energy harvesting by subcutaneous solar cells: a long-term study on achievable energy output," *Annals of biomedical engineering*, vol. 45, pp. 1172-1180, 2017, doi: 10.1007/s10439-016-1774-4.

[62] T. He, X. Guo, and C. Lee, "Flourishing energy harvesters for future body sensor network: from single to multiple energy sources," *IScience*, vol. 24, no. 1, 2021, doi: 10.1016/j.isci.2020.101934.

[63] G. Rong, Y. Zheng, and M. Sawan, "Energy solutions for wearable sensors: A review," *Sensors*, vol. 21, no. 11, 2021, doi: 10.3390/s21113806.

[64] T. Zhang *et al*., "Recent progress in hybridized nanogenerators for energy scavenging," *Iscience*, vol. 23, no. 11, 2020, doi: 10.1016/j.isci.2020.101689.

[65] A. S. Afroz, D. Romano, F. Inglese, and C. Stefanini, "Towards bio-hybrid energy harvesting in the real-world: pushing the boundaries of technologies and strategies using bio-electrochemical and biomechanical processes," *Applied Sciences*, vol. 11, no. 5, 2021, doi: 10.3390/app11052220.

[66] Y. Zou, L. Bo, and Z. Li, "Recent progress in human body energy harvesting for smart bioelectronic system," *Fundamental Research*, vol. 1, no. 3, pp. 364-382, 2021, doi: 10.1016/j.fmre.2021.05.002.

[67] J. Li, F. Yang, and X. Wang, "Respiration-driven triboelectric nanogenerators for biomedical applications," *EcoMat*, vol. 2, no. 3, 2020, doi: 10.1002/eom2.12045.

[68] E. Pourshaban *et al*., "A Magnetically-Coupled Micromachined Electrostatic Energy Harvester Driven by Eye Blinking Motion," *2021 21st International Conference on Solid-State Sensors, Actuators and Microsystems (Transducers)*, pp. 960-963, 2021, doi: 10.1109/Transducers50396.2021.9495499.

[69] X. Pu *et al*., "Wearable triboelectric sensors for biomedical monitoring and human-machine interface," *Iscience*, vol. 24, no. 1, 2021, doi: 10.1016/j.isci.2020.102027.

[70] L. L. Ruiz *et al*., "Piezoelectric-Based Respiratory Monitoring: Towards Self-Powered Implantables for the Airways," *2021 IEEE 17th International Conference on Wearable and Implantable Body Sensor Networks (BSN)*, pp. 1-5, 2021, doi: 10.1109/BSN51625.2021.9507022.

[71] A. Altan and R. Hacıoğlu, "Model predictive control of three-axis gimbal system mounted on UAV for real-time target tracking under external disturbances," *Mechanical Systems and Signal Processing*, vol. 138, 2020, doi: 10.1016/j.ymssp.2019.106548.

[72] E. Belge *et al*., "Estimation of small unmanned aerial vehicle lateral dynamic model with system identification approaches," *Balkan Journal of Electrical and Computer Engineering*, vol. 8, no. 2, pp. 121-126, 2020, doi: 10.17694/bajece.654499.

[73] S. Sarkar *et al*., "The mechanical properties of infrainguinal vascular bypass grafts: their role in influencing patency," *European journal of vascular and endovascular surgery*, vol. 31, no. 6, pp. 627-636, 2006, doi: 10.1016/j.ejvs.2006.01.006.

[74] H. D. M. Mayck *et al*., "A human heartbeat frequencies based 2-DOF piezoelectric energy harvester for pacemaker application," *Energy Harvesting and Systems*, vol. 8, no. 1, pp. 1-11, 2021, doi: 10.1515/ehs-2021-0011.

[75] M. G. Abdelmageed *et al*., "Design and simulation of pulsatile blood flow energy harvester for powering medical devices," *Microelectronics Journal*, vol. 86, pp. 105-113, 2019, doi: 10.1016/j.mejo.2019.02.021.

[76] R. A. Bergman, A. K. Afifi, and R. Miyauchi, "Illustrated encyclopedia of human anatomic variation: Opus II: Cardiovascular system: Arteries. Head, Neck and Thorax," *Common Carotid Arteries*, 2013.

[77] J. Lockwood and N. Desai, "Central venous access," *British Journal of Hospital Medicine*, vol. 80, no. 8, 2019, doi: 10.12968/hmed.2019.80.8.C114.

[78] M. Pl, *Marino's the ICU book*, *4th Edition. Philadelphia: Lippincott Williams & Wilkins*, 2013.

[79] H. Dukka, M. W. Taal, and R. Bayston, "Potential clinical value of catheters impregnated with antimicrobials for the prevention of infections associated with peritoneal dialysis," *Expert Review of Medical Device*, vol. 20, no. 6, pp. 459–466, 2023, doi: 10.1080/17434440.2023.2205587.

[80] J. S. Hanson, "Sixteen Failures in a Single Model of Bipolar Polyurethane-insulated Ventricular Pacing Lead: A 44-Month Experience," *Pacing and Clinical Electrophysiology*, vol. 7, no. 3, pp. 389–394, 1984, doi: 10.1111/j.1540-8159.1984.tb04923.x

[81] A. A. A. Zayed *et al*., "Design procedure and experimental verification of a broadband quad-stable 2-DOF vibration energy harvester," *Sensors*, vol. 19, no. 13, 2019, doi: 10.3390/s19132893.

[82] A. Coccarelli, R. V. Loon, and A. Chien, "A Computational Pipeline to Investigate Longitudinal Blood Flow Changes in the Circle of Willis of Patients with Stable and Growing Aneurysms," *Annals of Biomedical Engineering*, vol. 52, pp. 2000–2012, 2024, doi: 10.1007/s10439-024-03493-1.

[83] Overview of materials for Polyethylene Terephthalate (PET), Unreinforced. Retrieved from: https://www.matweb.com/search/datasheet.aspx?MatGUID=a696bdcdff6f41dd98f8eec3599eaa20&ckck=1.

[84] H. Liu, C. J. Tay, C. Quan, T. Kobayashi and C. Lee, "Piezoelectric MEMS Energy Harvester for Low-Frequency Vibrations With Wideband Operation Range and Steadily Increased Output Power," in *Journal of Microelectromechanical Systems*, vol. 20, no. 5, pp. 1131-1142, 2011, doi: 10.1109/JMEMS.2011.2162488.

[85] H. Liu *et al*., "A scrape-through piezoelectric MEMS energy harvester with frequency broadband and up-conversion behaviors," *Microsystem technologies*, vol. 17, pp. 1747-1754, 2011, doi: 10.1007/s00542-011-1361-4.

[86] J. C. Y. Ngu *et al*., "A narrative review of the Medtronic Hugo RAS and technical comparison with the Intuitive da Vinci robotic surgical system," *Journal of Robotic Surgery*, vol. 18, no. 99, 2024, doi: 10.1007/s11701-024-01838-5.

[87] D. F. Untereker *et al*., "8 - Power Sources and Capacitors for Pacemakers and Implantable Cardioverter-Defibrillators," *Clinical Cardiac Pacing, Defibrillation and Resynchronization Therapy (Fifth Edition)*, pp. 251–266, 2017, doi: 10.1016/B978-0-323-37804-8.00008-0.